England (1957).
7. Cullen, E. J., and J. F. Davidson, *Chem. Eng. Sci.*, **6**, 49 (1956).
8. Danckwerts, P. V., and A. M. Kennedy, *Trans. Inst. Chem. Engrs. (London)*, **32**, S53 (1954).
8a. ————, Chem. Eng. Sci., **8**, 201 (1958).
9. Danckwerts, P. V., *Research*, **2**, 494 (1949).
10. Davidson, J. F., and E. J. Cullen, *Trans. Inst. Chem. Engrs. (London)*, **35**, 51 (1957).
11. Duda, J. L., and J. S. Vrentas, *Chem. Eng. Sci.*, **27**, 22 (1967).
12. Emmert, R. E., and R. L. Pigford, *Chem. Eng. Progr.*, **50**, 87 (1954).
13. Fairbanks, D. F., and C. R. Wilke, *Ind. Eng. Chem.*, **42**, 471 (1950).
14. Fedorovich, E. D., and W. M. Rohsenow, "Engineering Projects Laboratory," NSF GK-39 (May, 1968).
15. Fosberg, T. M., and W. J. Heideger, *Can. J. Chem. Eng.*, **45**, 82 (1967).
16. Govindan, T. S., and J. A. Quinn, *AIChE J.*, **10**, 35 (1964).
17. Harriott, Peter, *ibid.*, **6**, 528 (1960).
18. *Ibid.*, 708.
19. Heideger, W. J., and M. Boudart, *Chem. Eng. Sci.*, **17**, 1 (1962).
20. Hickman, K., "First International Symposium on Water Desalination," Washington, D. C. (Oct., 1965).
21. Higbie, Ralph, *Trans. Am. Inst. Chem. Engrs.*, **31**, 365 (1935).
22. Maa, J. R., *Ind. Eng. Chem. Fundamentals*, **504**, 6 (1967).
23. McKelvey, J. M., *AIChE J.*, **6**, 706 (1960).
24. Minkowycz, W. J., and E. M. Sparrow, *Intern. J. Heat Mass Transfer*, **9**, 1125 (1966).
25. Nakano, Yoshisuke, Chi Tien, and W. N. Gill, *AIChE J.*, **13**, 1092 (1967).
26. Quinn, J. A., and P. G. Jeannin, *Chem. Eng. Sci.*, **15**, 263 (1961).
27. Raimondi, Pietro, and H. L. Toor, *AIChE J.*, **5**, 86 (1959).
28. Schrage, R. W., "A Theoretical Study of Interface Mass Transfer," Columbia Univ. Press, New York (1953).
29. Scriven, L. E., and R. L. Pigford, *AIChE J.*, **4**, 439 (1958).
30. *Ibid.*, **5**, 397 (1959).
31. Sinfelt, J. H., and H. G. Drickamer, *J. Chem. Phys.*, **23**, 1095 (1955).
32. Sukhatme, S. P., and W. M. Rohsenow, *J. Heat Transfer*, **88c**, 19 (1966).
33. Tung, L. H., and H. G. Drickamer, *J. Chem. Phys.*, **20**, 10 (1952).
34. Ward, W. J., and J. A. Quinn, *AIChE J.*, **10**, 155 (1964).
35. *Ibid.*, **11**, 1005 (1965).
36. Dang, V. D., M.S. thesis, Clarkson College of Technology, Potsdam, N. Y. (May, 1968).

*Manuscript received August 23, 1968; revision received February 7, 1969; paper accepted March 10, 1969.*

# Spray Quenching

**JAN J. LASKOWSKI and WILLIAM E. RANZ**

**University of Minnesota, Minneapolis, Minnesota**

**A study was made of spray quenching by high velocity gas atomization. A mathematical model of both high and low temperature spray quenching was developed. Data were taken for proving the validity of the model.**

**Experiments were performed on a vertical downward flow of air-water in a 1.0 in. diameter tube. Injection was by either of two modes. The first was a set of six peripheral liquid jets projecting water perpendicularly into the high velocity airstream. The second mode of liquid injection was by means of a 360° peripheral, annular slot, which laid down a continuous wall film at the point of injection. Air velocities of 430 and 200 ft./sec. and liquid injection rates of from 150 to 1,200 ml./min. were studied. The following physical quantities were measured: liquid fluxes, wall film flow rates, drop size distributions, and median drop size. An attempt was made to measure gas temperature in a dense spray by using two different types of temperature probes, but only liquid temperatures could be detected. A comparison of data with published data and correlations was made.**

**The best quenching conditions obtained were a liquid-to-gas mass ratio of 0.25, a Sauter mean drop diameter of 45 $\mu$, and an indicated characteristic quench time of $10^{-3}$ sec.**

Spray quenching is the process of rapidly cooling a hot gas by a liquid spray. This is accomplished by injecting liquid into a high velocity gas stream. To date, very little has been published on spray quenching. These accounts are of a highly qualitative nature and give one the impression that spray quenching is more of an art than a science.

The intent of this work was to measure characteristic quench times to gain some insight into how a spray quenching operation may be controlled.

There are a number of practical applications of high velocity atomization and spray quenching. Spray quenching may be used to stop or freeze reactions. Concentrations of a high temperature equilibrium are recovered if cooling is so fast that reversal cannot occur (except on very long time scales). Spray quenching has present-day application in missile launch systems where, at the moment of take-off and for a short time afterwards, there is a rapid efflux of hot combustion gases directed at the launch pad. The pad must be cooled during this time, usually by a liquid spraying operation. High velocity atomization is encountered in ram jet engines where the performance of the flame stabil-

Jan J. Laskowski is with the IBM Corporation, Poughkeepsie, New York.

izing element is directly dependent on the fuel concentration. Fuel is injected upstream of the flame stabilizing element. The local concentration at the stabilizer is dependent on how the fuel was injected and on how the fuel distribution in air changes between the point of fuel injection and the flame stabilizing element. High velocity atomization in hot gas streams also finds application in spray drying operations.

Spray quenching is a complex process; therefore, it was necessary to study a single characteristic system. The system chosen was air-water flowing vertically downward in a 1.0-in. tube after a nozzle accelerated the air flow.

## THEORY: PHYSICAL RATE PROCESSES

### High Temperature Quench

Assuming that negligible reaction takes place and that there is no heat of reaction, the equation

$$\frac{-dT}{dt} = \frac{SU}{c_{pG}}(T - T_s) \tag{1}$$

can be written as a rough approximation of the gas temperature change during a spray quench. $T_s$, the surface temperature of the droplets, can be no higher than the boiling point.

For sprays, $S$ can be considered nearly constant as long as little evaporation takes place. For spherical particles

$$S = \frac{6R^*}{d_{32}\,\rho_L} \tag{2}$$

The Reynolds number $N_{Red}$ of a drop in a spray, based on the particle diameter and its relative velocity with respect to the gas, will be less than approximately $10^2$; if not, additional breakup will probably occur. The overall heat transfer coefficient can then be approximated by the correlation (*1*)

$$N_{Nud} = 0.37\ N_{Red}^{0.6}\ N_{Pr}^{1/3} \tag{3}$$

if $N_{Red} > 20$, and for smaller Reynold's numbers by the correlation (*1*)

$$N_{Nud} = 2 + 0.37\ N_{Red}^{0.6}\ N_{Pr}^{1/3} \tag{4}$$

The Nusselt number $N_{Nud} = U_{d21}/k_s$ is based on the surface-diameter median diameter. In general, $N_{Nud}$ will be of an order larger than 2 and less than 10; hence

$$U \approx C\frac{k_s}{d_{21}} \tag{5}$$

can be written as an approximation. $C$ is a Nusselt constant between 2 and 10, and $k_s$ is the thermal conductivity of the surface gas and vapor at temperature $T_s$. Here it is assumed that the gas phase presents the major resistance to heat transfer.

Assuming that a relatively high temperature gas is being quenched, the surface temperature $T_s$ of the drops can be approximated by the boiling point temperature $T_{bp}$ of the material which forms the drops (*2*).

In terms of a massive particle quench of a very hot gas or a quench that has the capacity to absorb great quantities of heat, the average particle temperature does not change enough to affect significantly the value of the heat transfer driving force $(T - T_s) \approx (T - T_{bp})$. It does not matter, within the chosen degree of error, whether the heat transferred from the gas is heating up the drop liquid or causing evaporation. However, evaporation will affect, to a considerable extent, the value of $k_s$, the thermal conductivity of the surface gas vapor mixture. Therefore, let any errors due to evaporation be absorbed in the constant $C$ of Equation (5).

By assuming that $N_{Re} < 100$ and that $T_s$ and $k_s$ are relatively constant, substitution of Equations (2) and (5) into Equation (1) results in

$$-\frac{dT}{dt} = \frac{6CR^*k_s}{\rho_L\, c_{pG}\, d_{31}^2}(T - T_s) \tag{6}$$†

Equation (6) with boundary conditions

$$T = T_o \quad \text{at} \quad t = 0 \tag{7}$$

can be solved to yield the solution

$$\frac{T - T_s}{T_o - T_s} = e^{-\frac{t}{t_e}} \tag{8}$$

where

$$t_e = \frac{\rho_L\, c_{pG}\, d_{31}^2}{6CR^*k_s} \tag{9}$$

represents a characteristic spray quench time.

If it is assumed that $k_s \approx 1 \times 10^{-4}$ cal./(sec.)(cm.)(°K.); $\rho_L \approx$ 1-g./cc.; $c_{pG} \approx 0.25$ cal./(g.)(°K.); $C \approx 6$; and $d_{31} = 10^{-2}$ cm.$(100\mu)$, then $t_e \approx 0.01/R^*$ sec.

Therefore, with an average diameter of $100\mu$ and $R^* = 10$, a spray quench time of the order of $10^{-3}$ sec. should be possible. If $R = 1$, then $t_e = 10^{-2}$ sec. By allowing an average diameter of $30\mu$, then with $R = 1$, a $10^{-3}$ sec. quench is once more possible.

To achieve a massive particle quench, the average gas temperature must change greatly for a small change in average particle temperature. By assuming negligible evaporation

$$\Delta T_G c_{pG} = R^*\ \Delta T_L c_{pL} \tag{10}$$

for concurrent contact of gas and spray.

---

† By definition (*3*)

$$d_{21} = \bar{x}_{sd} = \frac{\int_x^\infty x^2 f(x)\,dx}{\int_x^\infty x f(x)\,dx}$$

$$d_{32} = \bar{x}_{vs} = \frac{\int_x^\infty x^3 f(x)\,dx}{\int_x^\infty x^2 f(x)\,dx}$$

$$\therefore d_{21} \cdot d_{32} = \frac{\int_x^\infty x^3 f(x)\,dx}{\int_x^\infty x f(x)\,dx}$$

since by definition (*3*)

$$d_{31} = \bar{x}_{vd} = \sqrt{\frac{\int_x^\infty x^3 f(x)\,dx}{\int_x^\infty x f(x)\,dx}}$$

Thereby, $d_{21} \cdot d_{32} = d_{31}^2$.

Solving Equation (10) for $R^*$, we get

$$R^* = \frac{\Delta T_G}{\Delta T_L} \cdot \frac{c_{pG}}{c_{pL}} \tag{11}$$

Thus, if $(c_{pG}/c_{pL}) \approx 0.25$, then with $R^* \approx 0.1$, $\Delta T_G/\Delta T_L = 0.4$; with $R^* = 1$, $\Delta T_G/\Delta T_L = 4$; and with $R^* = 10$, $\Delta T_G/\Delta T_L = 40$. By assuming evaporation to the extent that $R^*$ is changed by 10% and S is changed by a negligible amount, then, with a latent heat of approximately $10^3$ B.t.u./lb., the effective value of the ratio $c_{pG}/c_{pL}$ becomes 0.0025. Now, with $R^* = 0.1$, a $\Delta T_G/\Delta T_L$ of 40 is obtainable; with $R^* = 1$, $\Delta T_G/\Delta T_L = 400$; and with $R^* = 10$, $\Delta T_G/\Delta T_L = 4{,}000$. Hence, massive particle quenches, assuming 10% evaporation, can be obtained at $1/100^{\text{th}}$ of the $R^*$ values required with no evaporation.

It should be noted that the heat transfer rate can always be treated on an individual drop basis. With $R^* = 1$, the drops are separated on the average by a distance equal to approximately seven drop diameters, and with $R^* = 10$, by approximately three drop diameters.

### Low Temperature Quench

For a high temperature quench, it is expected that $\Delta T_G/\Delta T_L$ will be of the order $10^2$ to $10^3$. However, model experiments were performed at low temperatures, and a theory was needed to interpret experimental results.

By considering the change in liquid temperature during a low temperature quench, and by relaxing the restriction of no change in liquid temperature (which was assumed for the case of a high temperature quench), the following equation can be written:

$$\frac{d}{dt}(T_{Go} - T_G)c_{pG} = \frac{d}{dt}(T_L - T_{Lo})R^* c_{pL} = h_c(T_G - T_L)S \tag{12}$$

One can speak of average temperatures because the gas tends to be mixed, and the radial temperature gradients in the drops are small (less than 10% temperature change from center to surface) for the present case (4). Using the definition of specific surface given by Equation (2) and the heat transfer coefficient in terms of nearly constant $N_{Nu_d}$, we can rewrite Equation (12) as

$$\frac{dT_L}{dt} = \left[\left(T_{Go} + \frac{R^* T_{Lo}\, c_{pL}}{c_{pG}}\right) - \left(\frac{c_{pL}}{c_{pG}} R^* + 1\right) T_L\right] \cdot \left(\frac{6k_s N_{Nu}}{d^2_{31}\, c_{pL}\, \rho_L}\right) \tag{13}$$

where $T_G$ has been eliminated, and $d_{21}$ and $d_{32}$ are transformed into $d_{31}$, as shown in the footnote to Equation (6).

Equation (13) and the boundary condition

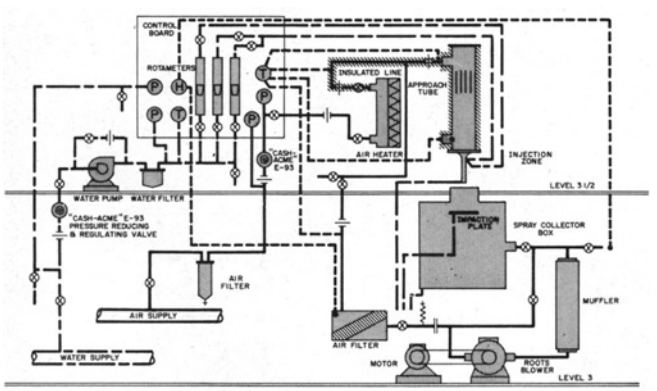


Fig. 1. Spray quenching equipment.

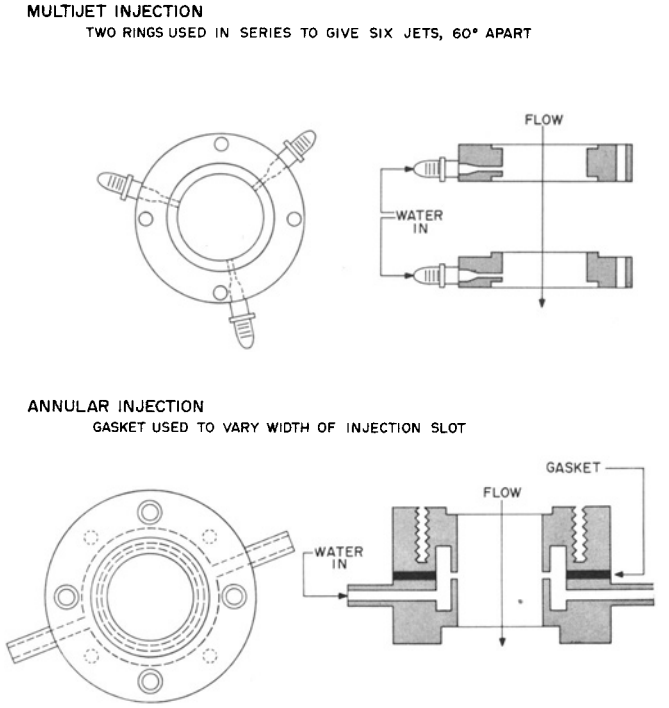


Fig. 2. Modes of liquid injection.

$$T_L = T_{Lo} \quad \text{at} \quad t = 0 \tag{14}$$

can be solved to yield the solution

$$\frac{T_L - \tau_L}{T_{Lo} - \tau_L} = \exp\left[\left(1 + \frac{R^* c_{pL}}{c_{pG}}\right)\left(\frac{k_s N_{Nu}}{c_{pL}}\right)\left(\frac{6}{d^2_{31}\, \rho_L}\right)\right] t \tag{15}$$

where

$$\tau_L = \frac{\left(T_{Go} + \dfrac{R^* c_{pL} T_{Lo}}{c_{pG}}\right)}{\left(1 + \dfrac{R^* c_{pL}}{c_{pG}}\right)} \tag{16}$$

By an analogous procedure, Equation (12) can be used to obtain an expression for the rate of change of the gas temperature $T_G$ with time:

$$\frac{T_G - \tau_G}{T_{Go} - \tau_G} = \exp\left[\left(1 + \frac{c_{pG}}{c_{pL} R^*}\right)\left(\frac{k_s N_{Nu}}{c_{pG}}\right)\left(\frac{6R^*}{d^2_{31}\, \rho_L}\right)\right] t \tag{17}$$

where

$$\tau_G = \frac{T_{Lo} + T_{Go}\left(\dfrac{c_{pG}}{c_{pL} R^*}\right)}{\left(1 + \dfrac{c_{pG}}{c_{pL} R^*}\right)} \tag{18}$$

$\tau_G$ represents the equilibrium temperature of the spray, or the temperature of the gas and liquid when they finally reach thermal equilibrium. $(T_{Go} - \tau_G)$ represents the difference between the initial gas temperature and the final gas temperature. The exponential (exp) group represents the rate at which the equilibrium gas temperature $\tau_G$ is reached. It can be seen that the characteristic quench time

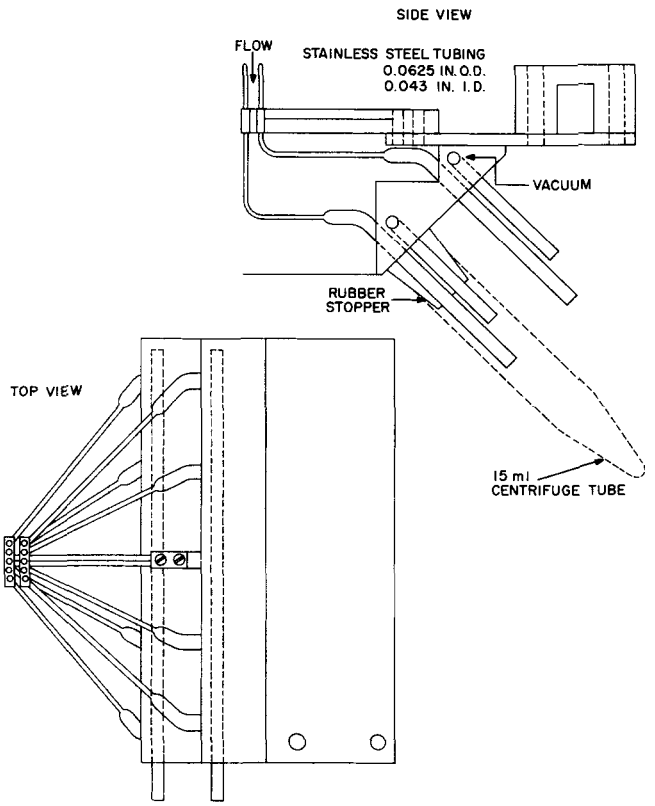


Fig. 3. Ten-probe flux sampler.

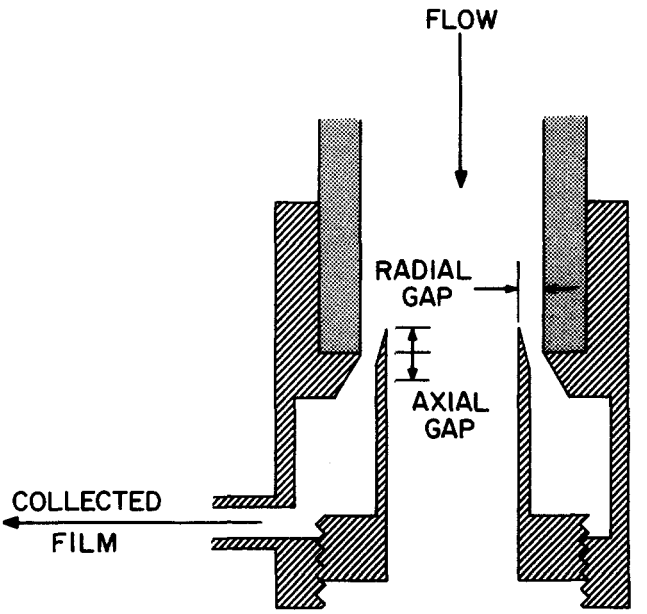


Fig. 4. Wall film skimmer.

for a relatively low gas temperature spray quench is proportional to $d^2_{31}/R^*$ as in the high temperature spray quench.

In a practical spray quenching system, to take advantage of the large effect of a small drop size, a high velocity gas stream of some sort would be utilized. To develop this high velocity gas stream, a converging nozzle with holdup time of order less than $10^{-3}$ sec. would be used. When we consider compressible, isentropic flow, there is a considerable temperature drop as a gas adiabatically flows from a reservoir through a converging nozzle. This temperature drop for an ideal gas is (5)

$$\frac{T_o}{T_f} = 1 + \frac{\kappa - 1}{2} N^2_{Ma} \qquad (19)$$

For the case of air, $\kappa = 1.4$, and at moderate Mach numbers of 0.4 to 0.6, the percentage drop in temperature going through a converging nozzle is of the order of 3 to 7%, respectively. Thus, the initial quench of chemical consequence may occur in the converging nozzle. The subsequent spraying of coolant serves only to maintain the cooler temperature.

It can be shown that first-order, reversible, chemical reactions with a rate constant as high as $10^4$ sec.$^{-1}$ can be quenched with less than a 10% loss in equilibrium product within a millisecond (6). Furthermore, the chemical quench is virtually completed within the first 20% of the possible decrease in gas temperature.

## EXPERIMENTAL EQUIPMENT

### Apparatus

A schematic diagram of the arrangement of the equipment utilized in the experimental investigations is shown in Figure 1.

The high velocity air was supplied by a blower and accelerated by a converging nozzle which met American Society of Mechanical Engineers standards. By regulating the blower inlet, the system could be run as a closed loop or open with ambient air being taken into the blower. A closed system was desired during the measurement of liquid flux, wall film flow rate, and drop size distribution to eliminate evaporation effects. The closed loop system was run until the recirculated air became saturated with water, and then experimental data were taken. In the case of temperature measurements, an open system was desired to see just what kind of quenching rates were achievable, evaporation effects included.

The output of air from the blower was regulated by using a bypass valve. After leaving the blower, the air was filtered and accelerated by the converging nozzle (4.0 to 1.0 in. diameter). Water was then injected to form a spray. The spray traveled downstream in a 1.0-in. tube and passed into a spray collector box with an impaction plate, where the drop size distribution could be determined and the liquid droplets separated from the air. In the case of a closed loop, the air was returned to the blower.

For temperature profile determinations, blower air was mixed with compressed air. The compressed air was filtered and heated in an electric heater before being mixed with the blower air at a point before the airstream entered the approach tube.

Injected water from the laboratory supply line was filtered, pumped (to maintain constant pressure), metered as to flow rate, pressure, and temperature, and then injected into the high velocity airstream.

Injection was by either of two modes. The first was a set of six peripheral liquid jets projecting water perpendicularly into the high velocity airstream. The jets were evenly spaced around the periphery of the tube. The second mode of liquid injection was by means of a 360 deg. peripheral, annular slot which laid down a continuous wall film at the point of injection. The slot width of this injector was variable. These two modes of water injection represented two opposite extremes. The multijet mode attempted to force all of the injected water to be suspended at the point of injection. The annular slot mode attempted to force all of the liquid to be on the wall of the tube, none suspended, at the point of injection. Figure 2 shows the two modes of liquid injection.

Various length 1.0 in. I.D. extension tubes were attached to the end of the converging nozzle. Data were taken from approximately 1.5 to 13.0 in. downstream from water injection. The investigation was not carried any further downstream because time scales of the order of 1 msec. were being considered. At the highest air velocity investigated, the airstream took approximately 2.5 msec. to go 13.0 in. downstream.

There was a Plexiglas* window at the top of the approach

* Trademark of Rohm and Haas Company.

tube so that the liquid injection zone could be visually observed from upstream.

An X-Y traversing mechanism was used to be able to locate any point in a radial cross-sectional plane to within ±0.01 in.

Air velocities were determined by making a nine point traverse downstream of the converging nozzle, with a hypodermic needle impact tube used.

### Liquid Flux

Liquid fluxes were determined by a sampling technique. A ten-probe sampler was used to take ten simultaneous liquid flow measurements at specific points within the spray over a particular time interval. The ten-probe sampler is shown in Figure 3. It was designed to give a large number of samples simultaneously without any single sampling probe interfering with the sampling of any other. The probes were designed to give greater than 98% capture efficiency for particles larger than 10$\mu$. A vacuum was drawn on the sampler to keep the tubes free flowing and to approximate isokinetic sampling. The sampler was placed in the spray, a fixed distance downstream from injection, facing upstream as shown in Figure 3. It can be shown that isokinetic sampling is not particularly critical at the air velocities under consideration here. The flux sampler was repositioned a number of times in each radial plane to achieve a complete flux profile (eighty-one points in 1.0 in. circular plane). Flux profiles were taken at various distances downstream from injection.

### Wall Film

To measure the flow of wall film at various distances downstream from injection, a wall film skimmer was designed. The wall film skimmer is shown in Figure 4. It removed all flow in the outer 0.04 in. of the tube (that is, the circular annular space between $r = 0.50$ in., the wall; and $r = 0.46$ in.). This quantity of liquid was defined as the wall film. The device worked well, with difficulty encountered only at relatively low airstream velocity (200 ft/sec.), where as much as 20% of the total liquid flowing escaped collection by streaming over the collection gap. The liquid streamed over at relatively few places rather than over the entire periphery and could easily be collected and corrected for. The gap width and lip overhang were varied and then fixed to give optimum results.

### Median Drop Size and Drop Size Distribution

Median drop size and drop size distribution were measured by a technique of inertial impaction. The spray was directed into the spray collector box, which contained an impaction plate. The plate and inlet diffuser created a two-dimensional stagnation flow.

A schematic of the inertial impaction system is shown in Figure 5. The distance between the diffuser outlet and the impaction plate could be varied by repositioning the impaction plate. At each position of the impactor plate, all droplets

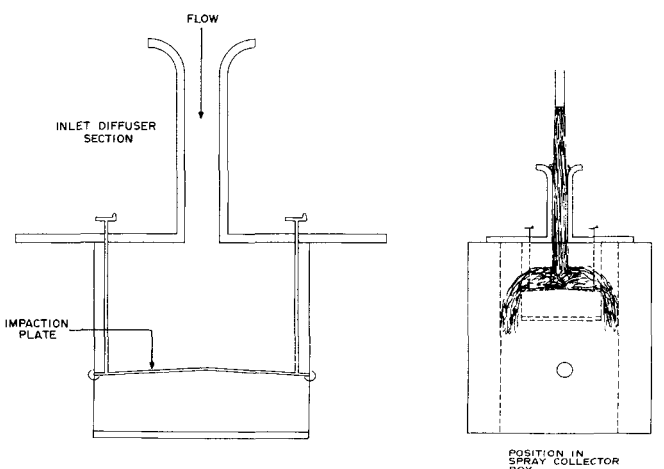


Fig. 5. Inertial impaction system.

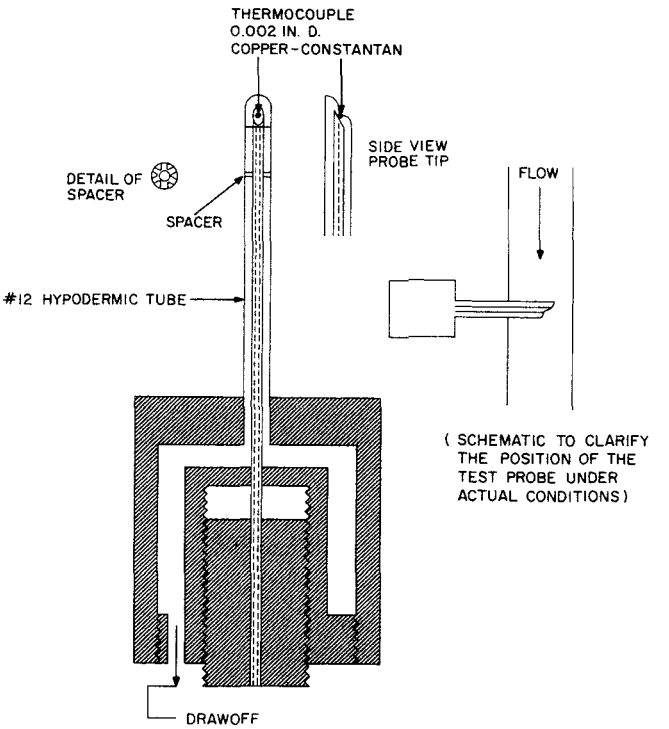


Fig. 6. Shield thermocouple temperature probe.

smaller than a certain characteristic diameter in the spray impacted on the plate and droplets larger escaped impaction. For each position of the impactor plate, there is a specific characteristic cut diameter. The closer the plate is to the diffuser outlet, the smaller is the characteristic diameter.

Measurement was made of the volume of the runoff from the impactor plate and the volume of the droplets that escaped impaction, which were separated from the flow in the spray collector box. By comparing these two volumes, and by knowing the characteristic diameter corresponding to that impaction plate position, the volume of the water in the spray with a droplet diameter less than the characteristic diameter could be calculated. By repositioning the impaction plate at other positions with different characteristic diameters, a drop size distribution could be generated. From the drop size distribution, a volume median drop diameter was obtained.

Drop size distributions were determined either relatively close to injection (3.0 in. extension tube between liquid injection and the spray diffuser inlet) and far downstream (13.0 in. extension tube).

Characteristic diameters for each impaction plate position were obtained from the test procedure established by Ranz and Hofelt (7). Correction factors were also applied to account for non-Stokes law behavior of the droplets.

Some problems with backflow and recirculation within the diffuser section were encountered when the impaction plate was close to the diffuser outlet; plate distance = 0.2 to 0.4 of the width of the diffuser. These difficulties are described and discussed in reference 6.

The wall film was skimmed off before the spray was allowed to enter the spray diffuser section of the spray collector box.

It is difficult to estimate the accuracy of the method, since no standard test exists with which to compare it. The method is rapid and gives an indicated drop size even for dense sprays such as encountered in this study of spray quenching. Droplet sizing of dense ($R_c > 0.01$) sprays by other methods has yet to prove successful.

### Temperatures

To investigate gas temperature profiles of a spray quench, two types of temperature probes were used. The first type of probe was modeled after the design of Benedict (8) and was of the sampling type. This probe was unsuccessful in obtaining gas or spray temperatures even in relatively sparse sprays of annular injection with low air velocities (6).

The second probe was of the more direct reading type. The

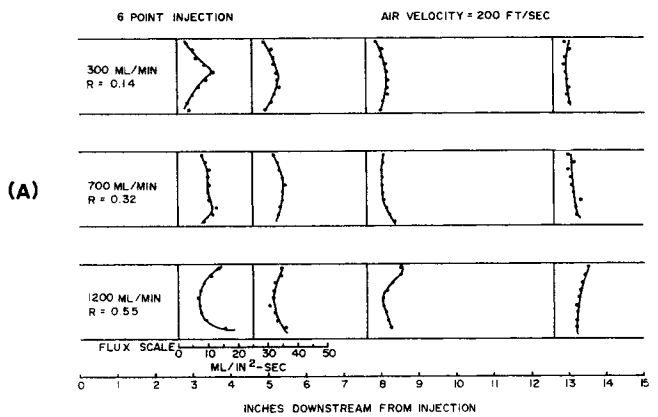


Fig. 7a. Center-line flux profiles: multijet injection, low airstream velocity.

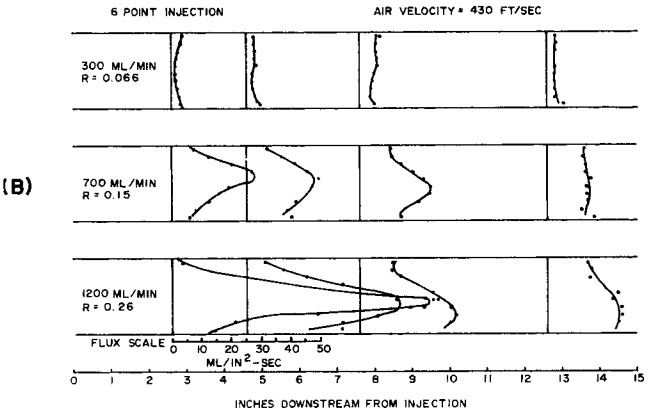


Fig. 7b. Center-line flux profiles: multijet injection. high airstream velocity.

temperature sensor was located within the spray, and a gas temperature was read under adverse conditions (that is, with water continually present). The design of the second probe is shown in Figure 6. A bare thermocouple was mounted at the end of a two-hole alumina insulator. The insulator was then placed in a tube whose end was shaped to protect the thermocouple from the spray gas stream. An adjustable suction rate of gas drawn between the alumina insulator and the outer tube removed any liquid that collected on or near the sensor and prevented any stagnation of gas or buildup of liquid near it.

During temperature profile determinations, the entire system was run open, with ambient air entering the blower. Blower air was mixed with heated laboratory compressed air and then passed into the liquid injection zone. Velocities could be matched with those achieved with a closed loop by the use of a bleed valve between the blower and the injection of hot compressed air.

Temperature readings were taken at various points in a radial plane and at various distances downstream from water injection.

## RESULTS AND CONCLUSIONS

### Liquid Flux

Flux measurements were made over a radial cross-sectional plane, approximately 3.0, 5.0, 8.0, and 13.0 in. downstream from either multijet or annular injection. Three water injection rates were investigated; 300, 700, and 1,200 ml./min.

For the case of multijet injection, axial plane profiles for the low air velocity are given in Figure 7*a*. The results for the high air velocity are given in Figure 7*b*.

For the low air velocity condition, flux profiles of varied shape were noted at the first test section (2.625 in. downstream from injection), depending on the initial injection rate. Observing the injection zone through the window at the top of the approach tube helped explain the profiles. At an injection rate of 300 ml./min., the liquid jets projected into the airstream approximately half to three-quarters the distance to the tube center. A center peaked liquid distribution within a short distance from injection is the result. At a liquid injection rate of 700 ml./min., it was observed that the six liquid jets seemed to join one another at the center of the tube. Owing to weak impingment and/or crossover, some of the liquid was thrown back towards the wall of the tube. The resulting flux profile a short distance from injection was flat, with a fairly even distribution of water across the tube. This would be desirable for uniform and rapid heat transfer. At a still higher liquid injection rate of 1,200 ml./min., there was a strong impinging of jets and/or crossover at the center of the tube, throwing a great deal of water back to the tube wall. This gave rise to a concave liquid distribution at a short distance from injection.

Flux profiles far downstream from injection were all fairly flat, independent of the initial rate of liquid injection. Turbulence produced a mixed, uniform liquid distribution within a relatively short period of time. At 200 ft./sec., the air took approximately 5 msec. to go 12.625 in.

For the high velocity condition (Figure 7*b*), there was also a wide variation in the shape of flux profiles a short distance downstream. At an initial water injection rate of 300 ml./min., a concave flux profile was measured. This was explained by observing the spray injection zone. At high air velocity and low liquid rate, the jets were unable to project into the airstream and were smeared along the

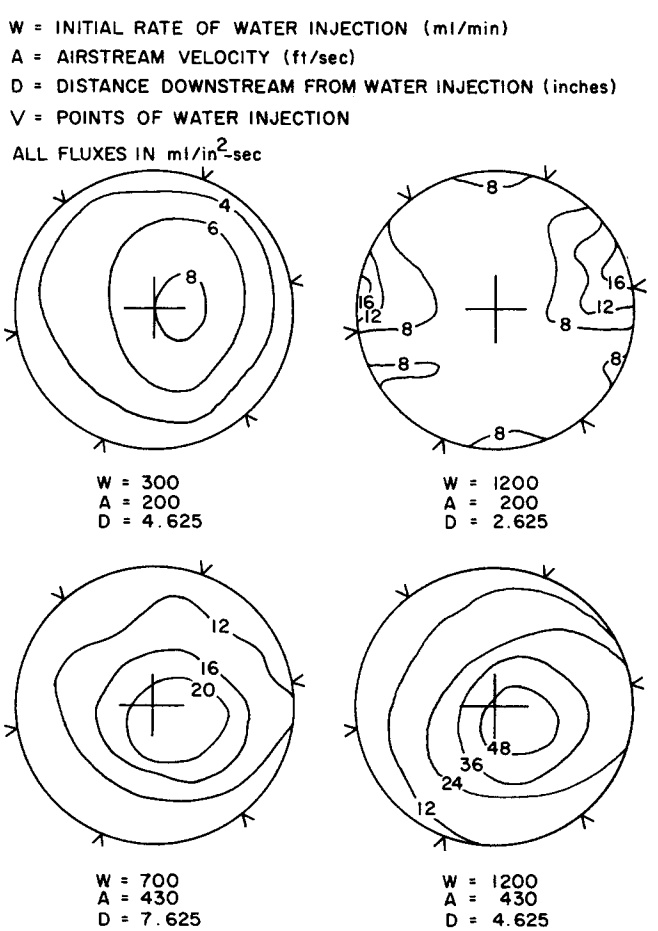


Fig. 8. Typical flux contours (radial cross sections, multijet injection).

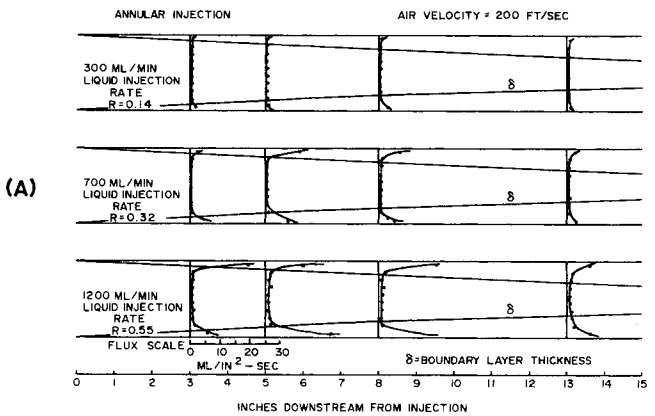


(A)

Fig. 9a. Center-line flux profiles: annular injection, low airstream velocity.

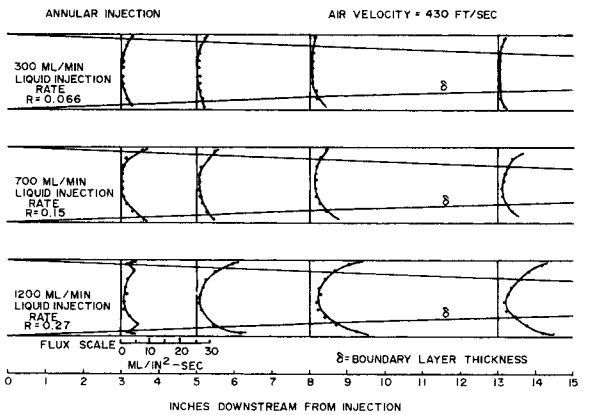


(B)

Fig. 9b. Center-line flux profiles: annular injection, high airstream velocity.

wall. It was difficult to pinpoint the exact water velocity at which the liquid jet was able to project, the best estimate being somewhere between 300 and 400 ml./min. liquid injection rate.

By applying criteria of balanced stresses, there are two conditions for a detached liquid jet. First, in order that liquid surface tension will not drag the jet down on the thin film which covers the wall near the orifice

$$\frac{\rho_L v_L^2/2g_c}{4\sigma_L/D_j} > K_1 \qquad (20)$$

for a detached jet. The second condition, in order that the trajectory of the jet does not bend on a radius of an order less than the jet diameter and bring the sides of the jet in contact with the wall

$$\frac{\rho_L v_L^2/2g_c}{\rho_G v_G^2/2g_c} > K_2 \qquad (21)$$

for a detached jet. Both Equations (20) and (21) are obtained by making a force balance on a jet issuing from a wall. To satisfy the observed conditions (at low velocity, detached jet occurs below liquid injection rate of 300 ml./min., and at high velocity, detached jet occurs between a liquid injection rate of 300 and 400 ml./min.), $K_1$ will have to be less than 3 (detachment, high or low air velocity at liquid injection rate of less than 300 ml./min.), and $K_2$ will be approximately equal to 1 (high velocity detachment at 330 ml./min. and low velocity detachment at 155 ml./min.).

At a liquid injection rate of 700 ml./min., the jets were able to project themselves into the airstream, approximately 0.25 in. or so from the wall. The result is a center peaked liquid distribution a short distance from injection. At a still larger liquid injection rate of 1,200 ml., the jets were well projected into the airstream, approximately 0.4 in. or so, but they were not quite impinging on one another. The result was a very sharply peaked flux profile a short distance downstream from initial injection. The peak in the liquid flux (approximately 90 ml./in.$^2$-sec.) is almost four times a uniform average based on the liquid injection rate (approximately 25 ml./in.$^2$-sec.). As in the case of the low air velocity, flux profiles far downstream from injection were fairly flat and uniform. Although the profile for an initial injection rate of 1,200 ml./min. was not yet flat at 12.625 in. downstream, the difference between it and the profile at 2.625 in. downstream was enormous. In the case of the high air velocity, the air took approximately 2.3 msec. to go 12.625 in.

Figure 8 gives some typical flux contour plots for radial cross sections (lines of constant liquid flux). These contour plots are built up by using best fit curves of the flux profiles. The effects of six finite points of injection can be seen only very close to injection. At 2.625 in. downstream from injection, an irregular set of flux contours is noted, but by 4.625 in. downstream, the effect of the finite points of injection is lost, and the flux contours become continuous and fairly symmetrical about the center point of the radial tube cross section. Slight asymmetry was noted and was expected in this highly turbulent airstream which had just undergone entrance, exit, and converging effects. With both the high and the low air velocities, the nonuniform mode of injection was no longer apparent at 4.625 in. downstream from injection.

Center line flux profiles for the annular mode of liquid injection, high and low air velocities are shown in Figures 9*a* and *b*. At the low air velocity (Figure 9*a*), very little water gets into the airstream; there is only a very weak dependence on the rate of liquid injection. Even at a liquid injection rate of 1,200 ml./min., no appreciable amount of water (less than 15%) is suspended in the airstream. The flux profile is very concave, with a water flux rapidly decreasing from the wall.

At the higher air velocity (Figure 9*b*), spray flux was increased only slightly. At the low liquid injection rate of 300 ml./min., no appreciable amount of water got into the airstream. At the higher liquid rates, 700 and 1,200 ml./min., the amount of water that became suspended was slightly better than for the same liquid injection rate and the low air velocity. The flux profiles far downstream from injection were still concave but not as severe as in the low velocity case. Close to injection almost no water was getting into the airstream. Apparently this is not a good way to get liquid quickly into the airstream and uniformly distributed.

The relatively high axial liquid flux near the wall and its rapid decrease toward the center of the tube in annular injection may be partially explained by a turbulent boundary layer that starts at the point of liquid injection. For turbulent boundary-layer growth over a flat plate that starts at the point $x = 0$ and has a boundary-layer thickness $\delta$ (defined as the point where velocity in the boundary layer equals the average free stream velocity), the following equation is available (9):

$$\delta = 0.37 \left(\frac{\mu_G}{\rho_G v}\right)^{1/5} x^{4/5} \qquad (22)$$

$x$ is the distance downstream from the point where the boundary layer starts, and $v$ is the average free stream

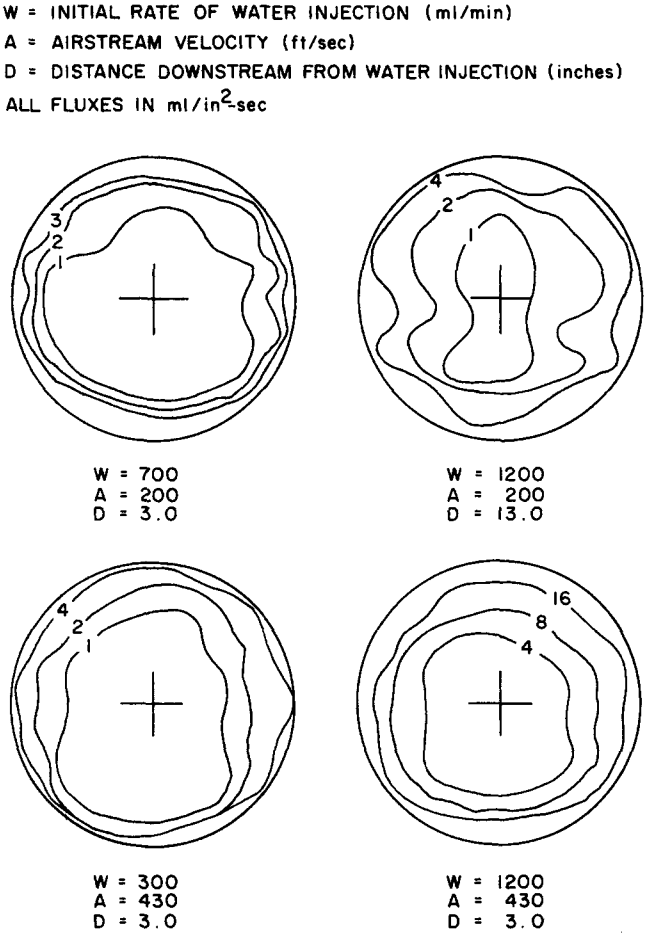


**Fig. 10. Typical flux contours (radial cross sections, annular injection).**

velocity.

The growth of such boundary layers, calculated for the conditions under which the annular flux data were taken, are also plotted in Figures 9*a* and *b*. Looking at these figures, one can see, especially for the low air velocity (Figure 9*a*), that the high liquid flux concentration occurs within the theoretically calculated turbulent boundary layer. For the high airstream velocity, this is not completely the case, and some projection must occur to get the liquid into the free stream. Projection of particles beyond the turbulent boundary layer is a reasonable possibility. A 50-$\mu$ particle, to travel 0.5 in. from the wall to the center of the tube, requires only an initial projection velocity of approximately 15 ft./sec. Thus, with annular injection, the suspended liquid appears to stay within a turbulent boundary layer, and only a small amount of liquid is projected into the main stream. The higher the airstream velocity, the greater the quantity of liquid that can project through the turbulent boundary layer from rapidly rising wave crests.

As might be expected, no extreme cases of asymmetrical radial liquid distribution were encountered for the annular mode of liquid injection. Figure 10 gives some typical radial cross sections with liquid flux contours.

The general shape of the axial flux profiles agreed with those published by Gill, Hewitt, and Hitchon (*10*).

The following conclusions were made concerning liquid flux:

1. In multijet injection, apparent juncture of the liquid jets at the center of the tube helps produce a uniform liquid distribution within a very short (1 msec.) period of time.

2. With high velocity airstreams, the liquid injected by a multijet technique becomes uniformly distributed and independent of initial injection rate within a relatively short time (5 msec. or less).

3. The annular mode of injection is a relatively slow process for getting water into and evenly distributed across a high velocity airstream and requires a very long pipe length to subject all the gas to a spray quench.

4. The initial nonuniform effects of multijet injection are very quickly averaged out and are no longer noticeable within a millisecond or so from injection.

5. For multijet injection, the maximum $R^*$ achieved was 0.255 mass water/mass air. For annular injection, the maximum $R^*$ achieved was approximately 0.07.

### Wall Film Flow Rate

Wall film flow rates were determined over the same range of variables for which liquid fluxes were measured. In the case of annular injection, the effect of varying injection slot width was also investigated.

In the case of multijet injection, the rate of flow of the wall film as a function of the distance downstream from injection is shown in Figure 11*a* for the low velocity airstream and in Figure 11*b* for the high velocity airstream. It can be seen that there is a considerable dependence of the wall film flow rate on the airstream velocity. At a high air velocity (Figure 11*b*), the wall film builds up as it travels downstream from injection. The greater the initial rate of water injection, the greater the rate of buildup of the film. This is not at all true for the lower air velocity studied (Figure 11*a*). There is little change in the wall film flow rate as it travels downstream from injection. It appears as though at an air velocity of 200 ft./sec., a wall film is very quickly set up (within 2.5 in. or less of injection), and then it changes very slowly as it moves downstream. At an air velocity of 430 ft./sec., the airstream is able to hold the water injected in a suspended state for a much longer period of time, and the wall film is still drastically changing. This is especially true at high water injection rates far downstream from injection (12.625 in.).

Figure 12 shows how the relative distribution of liquid between the wall film and airstream changes as a function of water injection rate at 2.625 and 12.625 in. downstream from injection. The atomization efficiency (A.E.) is defined as the percentage of the total water injected in the form of a suspended spray. The percentage of the injected water flowing in the wall film is 100-atomization efficiency. For the high velocity airstream, the atomization efficiency increases as the water injection rate is increased, reaches a peak, and subsequently decreases. The maximum atomization efficiency (the peak) occurs at smaller liquid injection rates farther from injection. At high air velocity, the advantageous condition of high atomization efficiency ($\geq$90%) at high liquid injection rates (600 to 1,200 ml./min.) and at a very short distance from injection (2.625 in.) is encountered.

At low air velocity, a strange effect was noted. Here, a strong maximum peak in the atomization efficiency occurred at approximately 300 to 400 ml./min. water injection rate. The peak became less pronounced at sections farther downstream from injection, but it was still appreciable at 12.625 in. It was only at the water injection rates for this maximum that the low air velocity could compete with the high air velocity in getting a large amount of water suspended.

The most probable explanation for this maximum is impinging and/or crossover of the jets at the center line of

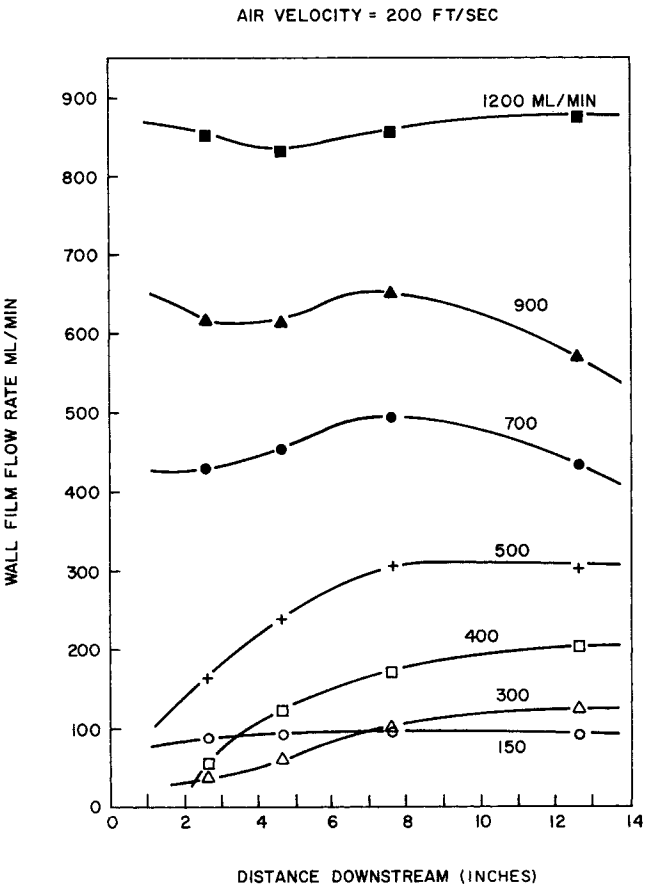


Fig. 11*a*. Wall film flow rate as a function of distance downstream from multijet injection for various initial water injection rates, low airstream velocity.

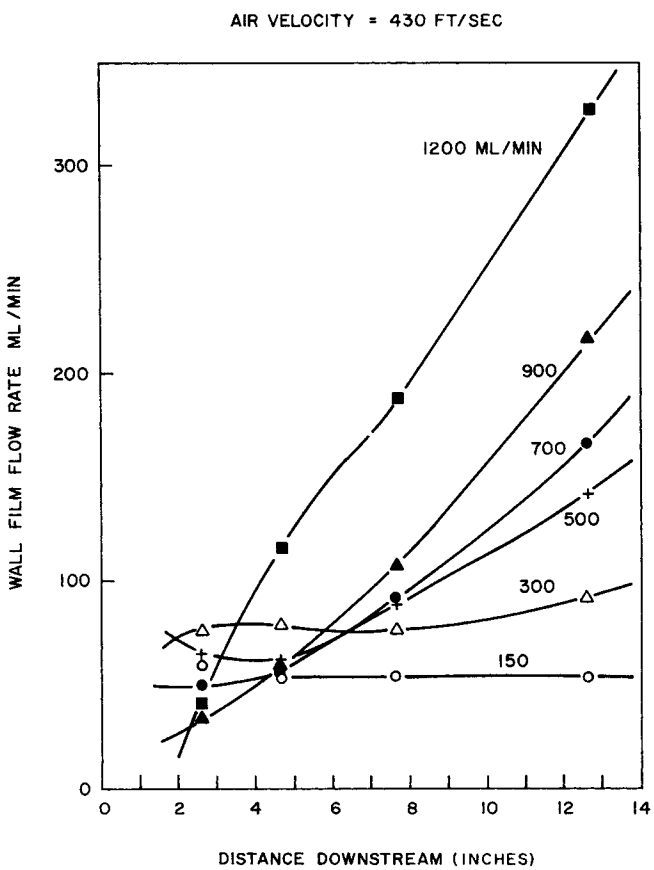


Fig. 11*b*. Wall film flow rate as a function of distance downstream from multijet injection for various initial water injection rates, high airstream velocity.

the tube. At a water injection rate of 300 ml./min., the jets appeared to project to approximately 0.25 in. from the wall. At 700 ml./min. water rate, the jets seemed to impinge on one another at the center of the tube. It was difficult to specify the exact liquid rate at which the jets met at the center of the tube, with an estimate being somewhere between 500 and 600 ml./min. water injection rate at the low air velocity. Thus, the maximum in the atomization efficiency represents a condition where the jets are still atomizing as single separate units. As the water injection rate is increased from this point, interference, coalescence, crossover, and impaction on the opposite walls all tend to occur, and the atomization efficiency decreases. In the previous section, it was shown that the interaction and impinging of jets tended to give a uniform flux distribution across the tube. In the case of wall film flow rates, it was shown that intersecting jets tend to decrease the atomization efficiency of the system. However, with the atomization efficiency decreasing, one can still have as much or more water (suspended) on an absolute basis. For instance, at 350 ml./min., there was 80% suspended or 280 ml./min. suspended. At 1,000 ml./min., there was 30% suspended or 300 ml./min. suspended.

Wall film flow rates as a function of distance downstream from annular injection are given in Figures 13*a* and *b*. The data shown in Figures 13*a* and *b* were produced by a 5 mil annular slot. Corresponding data were taken by

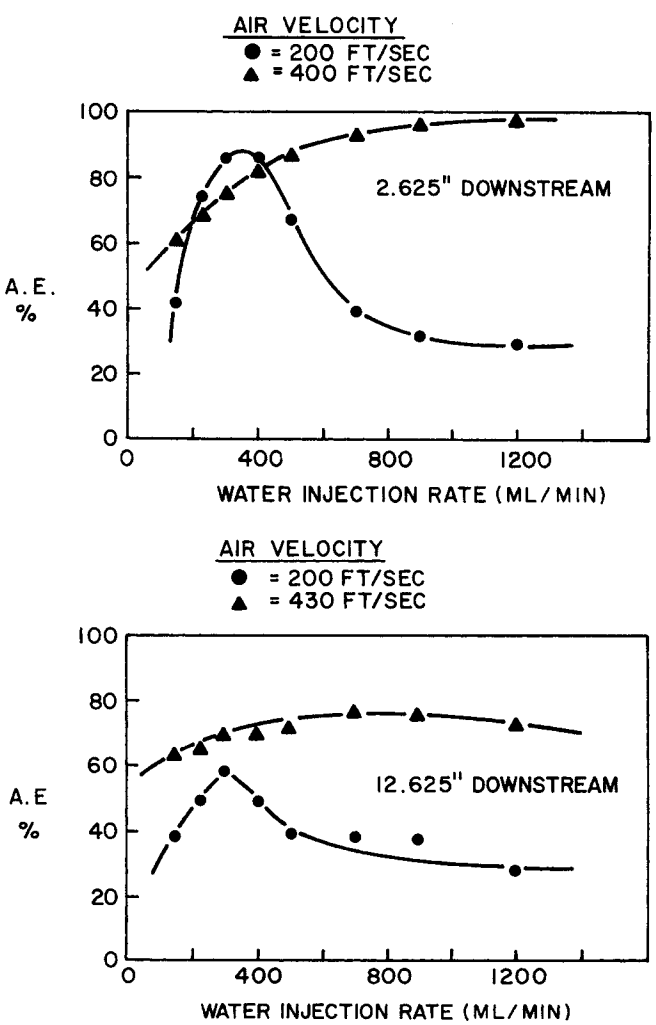


Fig. 12. Atomization efficiency as a function of rate of liquid injection by multijets at various distances downstream from initial injection.

TABLE 1. RESULTS, DROP SIZE DISTRIBUTIONS AND SAUTER MEAN DIAMETER

Multijet injection

| Water injection rate, ml./min. | Wall film flow rate, ml./min. | Distance downstream from injection, in. | Temperature Water °F. | Temperature Air, °F. | $d_{VMD}$, $\mu$ | Std. dev. $\sigma$, $\mu$ | Rel. std. dev., $\sigma_g$ | $d_{32}$, $\mu$ |
|---|---|---|---|---|---|---|---|---|
| Air velocity = 200 ft./sec. | | | | | | | | |
| 300 | 40 | 2.625 | 74 | 78 | 82 | 40 | 0.49 | 76 |
| 300 | 125 | 12.625 | 75 | 87 | 92 | 65 | 0.71 | 85 |
| 700 | 430 | 2.625 | 73 | 77 | 104 | 92 | 0.88 | 85 |
| 700 | 435 | 12.625 | 72/73° | 80/74° | 83/82° | 40/35° | 0.48/0.43° | 77/77° |
| 1,200 | 852 | 2.625 | 74 | 78 | 112 | 85 | 0.76 | 95 |
| 1,200 | 875 | 12.625 | 76 | 85 | 96 | 60 | 0.63 | 85 |
| Air velocity = 430 ft./sec. | | | | | | | | |
| 300 | 76 | 2.625 | 79/72° | 90/89° | 77/77° | 70/80° | 0.91/1.04° | 62/60° |
| 300 | 94 | 12.625 | 76 | 103 | 55 | 42 | 0.76 | 47 |
| 700 | 50 | 2.625 | 75/73° | 87/87° | 133/138° | 410/400° | 3.08/2.90° | 49/55° |
| 700 | 168 | 12.625 | 76 | 101 | 65 | 67 | 1.03 | 51 |
| 1,200 | 41 | 2.625 | 72/73° | 85/88° | 152/163° | 550/640° | 3.62/3.92° | 47/46° |
| 1,200 | 330 | 12.625 | 80 | 108 | 74 | 75 | 1.01 | 58 |

° Two complete runs were made.

using a 10 mil annular slot. At the low air velocity (200 ft./sec.), there was a difference between the wall film flow rates, comparing the two slot widths, of less than 10%, and the difference averaged less than 4% over all of the data taken. At the high air velocity (430 ft./sec.), there was a maximum difference of 50% (at low liquid rates), and the difference averages less than 5% overall.

Figures 13*a* and *b* give similar results for wall film flow rates at the higher airstream velocity. Again, by comparing the two figures, the effect of annular slot width on wall film flow rates is slight. At lower liquid rates, there was more of a difference between the two slot widths than was encountered under similar conditions with low velocity air. At higher liquid injection rates ($\geq$ 700 ml./min.), the average difference between wall film flow rates for the two slot widths averaged less than 5% over all of the data taken. Again, as in the low air velocity case, a relatively small amount of water was suspended in the airstream within 13.0 in. of injection, but there is a threefold increase over the low air velocity case. Where this liquid was suspended is shown in Figure 10.

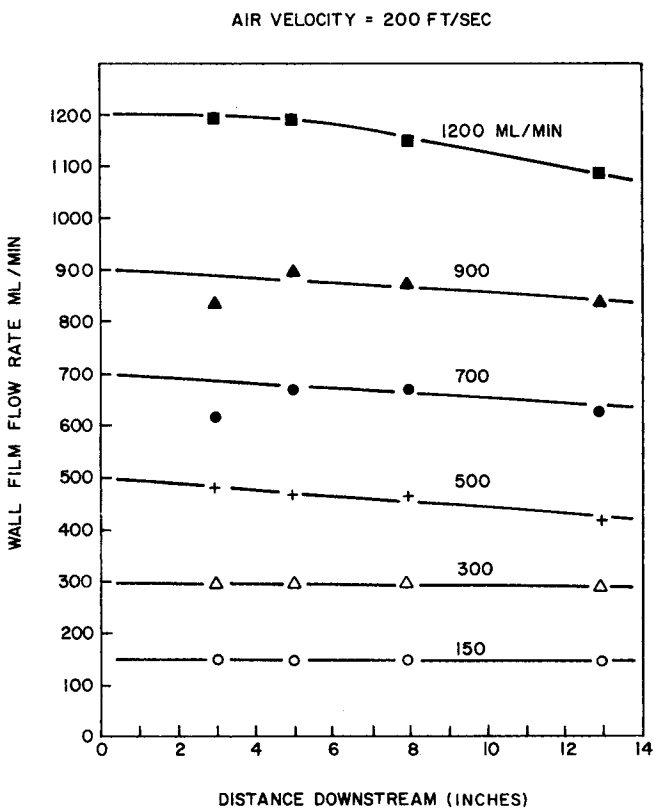


**Fig. 13*a*. Wall film flow rate as a function of distance downstream from 5-mil annular slot injection for various initial water injection rates, low airstream velocity.**

Figure 14 presents atomization efficiency as a function of water injection rate at 3 and 13 in. downstream from initial annular injection. At the high airstream velocity, the atomization efficiency decreases apparently to some asymptotic value. This asymptotic value increases slightly at sections farther and farther downstream, apparently toward some other asymptote with respect to downstream distance. A slight difference due to annular slot width can be seen, especially at the lower liquid injection rates.

At the lower air velocity, the atomization efficiency was always very low and difficult to measure. In no case did it go much above 15% and, in general, ranged below 15%. Even far downstream from injection (13 in.), no more than 20% of the water became suspended.

The following conclusions were made concerning wall film flow rate:

1. Multijet injection appears to be far superior to annular injection for suspending as much spray as possible in a short length of quench section and for having little wall film flow.

2. The wall film flow rate for multijet and annular injection is highly sensitive to airstream velocity. The higher the airstream velocity, the lower the wall film flow rate. The dependence on airstream velocity is relatively more pronounced with multijet injection than with annular injection.

3. Slot width of an annular injector has very little effect on the wall film flow rates.

4. At high air velocities, multijet injection has the desirable combination of high atomization efficiency for high

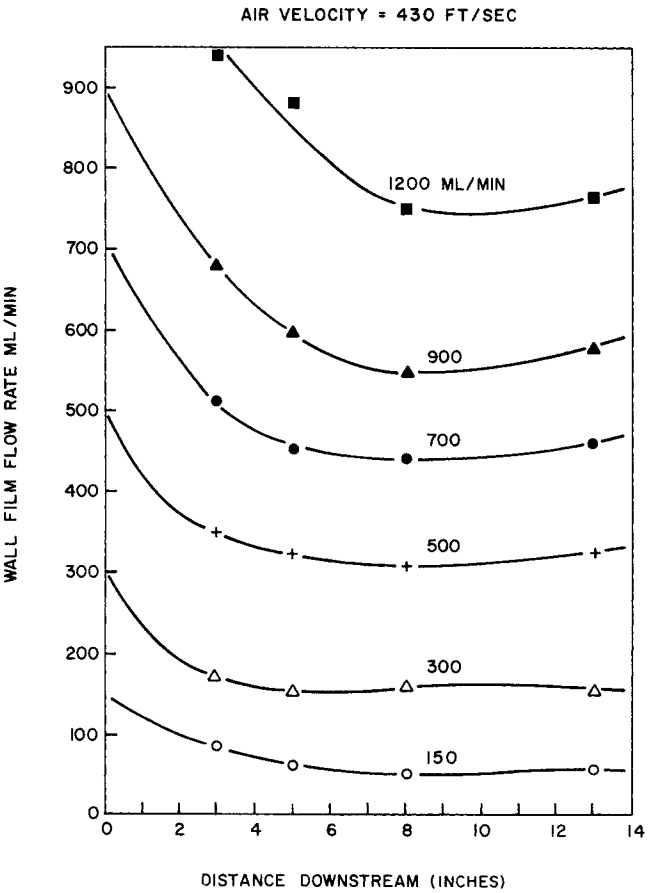


**Fig. 13b. Wall film flow rate as a function of distance downstream from 5-mil annular slot injection for various initial water injection rates, high airstream velocity.**

water injection rates at distances very close to water injection.

5. Apparent impinging of the multijets upon each other is detrimental towards keeping water suspended and decreases the atomization efficiency.

#### Drop Size Distributions

Drop size distributions were determined close to (2.0 to 3.0 in.) and far downstream (12.0 to 13.0 in.) from water injection for the following range of variables: water injection rate, 300, 700, and 1,200 ml./min.; multijet injection to high (430 ft./sec.) and low (200 ft./sec.) velocity airstreams; and 10 mil annular slot injection to a high velocity airstream. Because too small an amount of water becomes atomized, no determinations were made at the low airstream velocity for annular injection.

Figure 15 shows two typical drop size distribution determinations. The obviously bad datum point in each distribution was a result of the impaction plate being too close to the exit of the spray diffuser section, causing backflows in the inlet diffuser.

For multijet injection (Table 1), volume median droplet diameters $d_{VMD}$ for water injection into the low velocity airstream were found to be of the order 82 to 112$\mu$ and showed very little change in size while traveling downstream from injection. At the low water injection rate, there was a slight increase in volume median drop diameter as the spray traveled downstream. At the medium and high water injection rates, a slight decrease in the volume median drop size was noted downstream. These same trends were also true in the case of the calculated volume surface or Sauter, $d_{32}$, mean diameter. There was relatively little change in the median drop diameter with changing water injection rate. Close to injection, the median drop size increased slightly with increasing liquid injection rate. The relative standard deviations of the drop size distributions were from 0.4 to 0.9.

In general, multijet injection into the low velocity airstream produced volume surface mean drop diameters of the order 80 to 90$\mu$.

With multijet injection and the high air velocity, the volume median drop diameters were found to be sensitive to liquid injection rate; this was especially true for the spray from the section very close to water injection. The volume median droplet diameter 2.625 in. downstream from injection varied from 77 to 135 to 160$\mu$ as the liquid injection rate was increased from 300 to 700 to 1,200 ml./min. The relative standard deviation of the drop size distributions also increased with increasing water injection rate. As a result, the volume surface, or Sauter ($d_{32}$), mean diameter changed very little with water injection rate at a section relatively close to injection. At a section farther downstream (12.625 in.) from injection, the volume median and volume surface mean drop size increased slightly with increased liquid injection, but by no means in the proportions that the volume median size changed close to injection. The change in the volume median drop size is significant, especially at high liquid rates, as the spray travels downstream in the high velocity airstream. At 300 ml./min. water injection rate, the volume median drop diameter changes from 77 to 55$\mu$ within

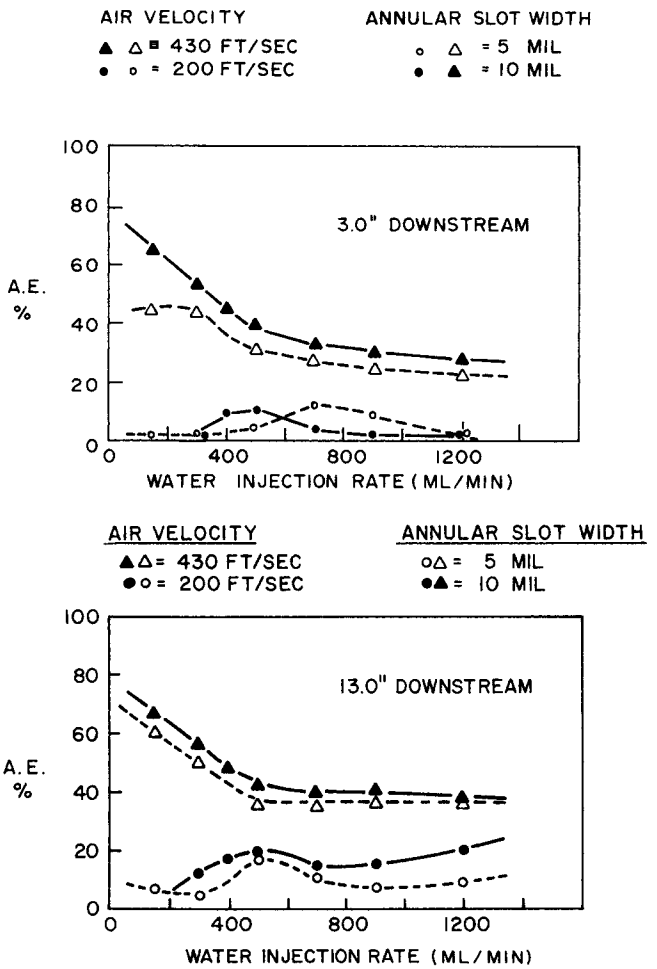


**Fig. 14. Atomization efficiency as a function of rate of liquid injection from 5- and 10-mil annular slots at various distances downstream from initial injection.**

10.0 in. (2.625 to 12.625 in. downstream). At 700 ml./min., it changes from 135 to 65$\mu$ and at 1,200 ml./min., from 158 to 74$\mu$ within 10.0 in. Thus, breakup is still occurring as the spray travels downstream. It is also possible that the larger droplets are migrating to the wall, impacting, and becoming part of the wall film. Looking back at Figure 11*b*, we can see that there is considerable change in the wall film flow rate between 2.625 and 12.625 in. downstream, especially at the higher liquid injection rates.

It is emphasized that when speaking of 2.625 or 12.625 in. downstream, one is speaking of the spray issuing from 2.625 or 12.625 in. extension tubes into the diffuser inlet to the impaction plate and the spray collector box.

In general, multijet injection with the high air velocity produced a volume surface (Sauter) mean drop diameter of 50 to 60$\mu$.

For the case of annular injection and the high velocity airstream (Table 2), the volume median and volume surface median drop diameters were found to be insensitive to the rate of liquid injection and to the distance downstream from injection. The volume median diameters were lower than those encountered with multijet injection. The drop size distributions were much more peaked than those with multijet injection. The relative standard deviation was approximately 0.3. In general, the annular mode of injection gives volume surface (Sauter) median drop diameters of the order 40 to 50$\mu$.

Mean drop size resulting from pneumatic atomization may be predicted by the Nukiyama and Tanasawa (*11*) empirical correlation (not dimensionally consistent), which is

$$d_{32} = \bar{x}_{vs} = 585 \frac{\sqrt{\sigma_L}}{v\sqrt{\rho_L}} + 597 \left(\frac{\mu_L}{\sqrt{\sigma_L \rho_L}}\right)^{0.45} \left(\frac{1{,}000\, Q_L}{Q_A}\right)^{1.5} \quad (23)$$

Although the Nukiyama/Tanasawa equation is based on data taken at much lower $R$ values than those used in this study, the correlation can apparently be extrapolated to a limited extent into the denser spray region. With the low airstream velocity (multijet injection), the Nukiyama/Tanasawa correlation did predict Sauter mean drop diameters within 10% of those measured. With the high velocity airstream and multijet injection, prediction was within an average of 25% and in no case worse than 55% of the measured values. With annular injection and the high velocity airstream, the difference between the Nukiyama-Tanasawa correlation and the measured Sauter mean drop size averaged 25% and in no case was greater than 30%.

The following conclusions were reached concerning the drop size distributions:

1. Annular injection produces a relatively sharper peaked drop size distribution and a relatively smaller volume median drop size than the multijet technique at the same conditions.
2. At the lower air velocity, multijet injection produces a spray with a median drop size, both volume and volume surface (Sauter), that is, relatively insensitive to rate of liquid injection and distance downstream from injection.
3. At the high air velocity, multijet injection produces a spray with a volume median drop size that increases with increasing liquid injection rate and decreases with distance from injection. The Sauter mean drop size, on the other hand, proves to be relatively insensitive to liquid injection rate and distance downstream when compared with the volume median diameter.
4. At the high air velocity, annular slot injection produces a median drop size, both volume and volume surface (Sauter), that is relatively insensitive to liquid rate and distance downstream from injection.
5. At the high air velocity with multijet injection, drop breakup continues after initial injection as the spray travels downstream. This is not true for annular injection and multijet injection with the low velocity airstream.
6. The Nukiyama-Tanasawa (*11*) correlation for Sauter mean drop diameter can be used for prediction of mean drop size even for the dense spray conditions studied in this investigation.

#### Temperature Profiles

Indicated temperature profiles were taken by using both the concentric tube removal probe and the shielded tip thermocouple probe for the multijet and annular slot modes of water injection. Data were taken for the high (430 ft./sec.) and low (200 ft./sec.) velocity airstream and four water injection rates, 300, 500, 700, and 1,200 ml./min. Temperature was measured at the center line of the tube for various distances downstream from slightly over 1.0 in. from injection to over 12.0 in. downstream. Temperatures were also measured axially downstream at a point halfway in from the wall to the center (one-quarter the tube diameter). For the multijet injection mode, the halfway temperature measurement was made either directly below a point of injection (position A in Figure 16*a*) or directly below, equidistant from two points of injection (position B in Figure 16*a*). For the annular injection mode, the point on the tube wall circumference for the temperature measurement halfway in toward the center was chosen at random because the injection was continuous around the

Table 2. Results, Drop Size Distributions and Sauter Mean Diameter

Annular slot injection

| Water injection rate, ml./min. | Wall film flow rate, ml./min. | Distance downstream from injection, in. | Temperature, Water, °F. | Temperature, Air, °F. | $d_{VMD}$, $\mu$ | Std. dev. $\sigma$, $\mu$ | Rel. std. dev., $\sigma_g$ | $d_{32}$, $\mu$ |
|---|---|---|---|---|---|---|---|---|
| Air velocity = 430 ft./sec. | | | | | | | | |
| 300 | 140 | 3.0 | 80 | 83 | 52 | 15 | 0.29 | 50 |
| 300 | 136 | 13.0 | 75 | 95 | 48 | 12 | 0.25 | 47 |
| 700 | 485 | 3.0 | 76 | 92 | 52 | 15 | 0.29 | 50 |
| 700 | 425 | 13.0 | 72 | 98 | 52 | 15 | 0.29 | 50 |
| 1,200 | 870 | 3.0 | 80/73* | 83/84* | 50/48* | 36/20* | 0.72/0.42* | 43/45* |
| 1,200 | 750 | 13.0 | 75 | 95 | 53 | 17 | 0.32 | 51 |

* Two complete runs were made.

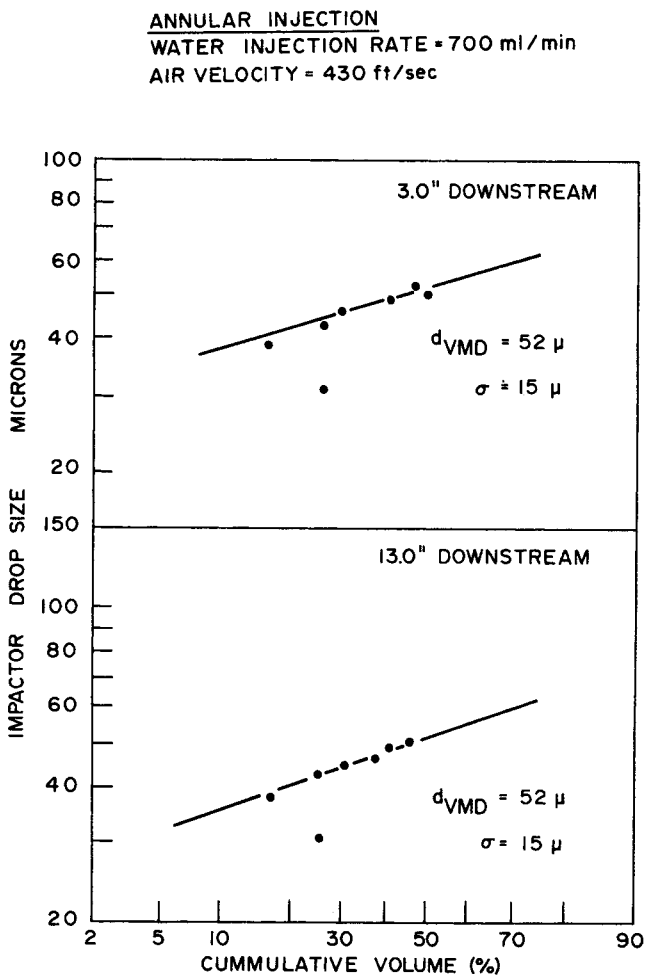


Fig. 15. Typical drop size distributions.

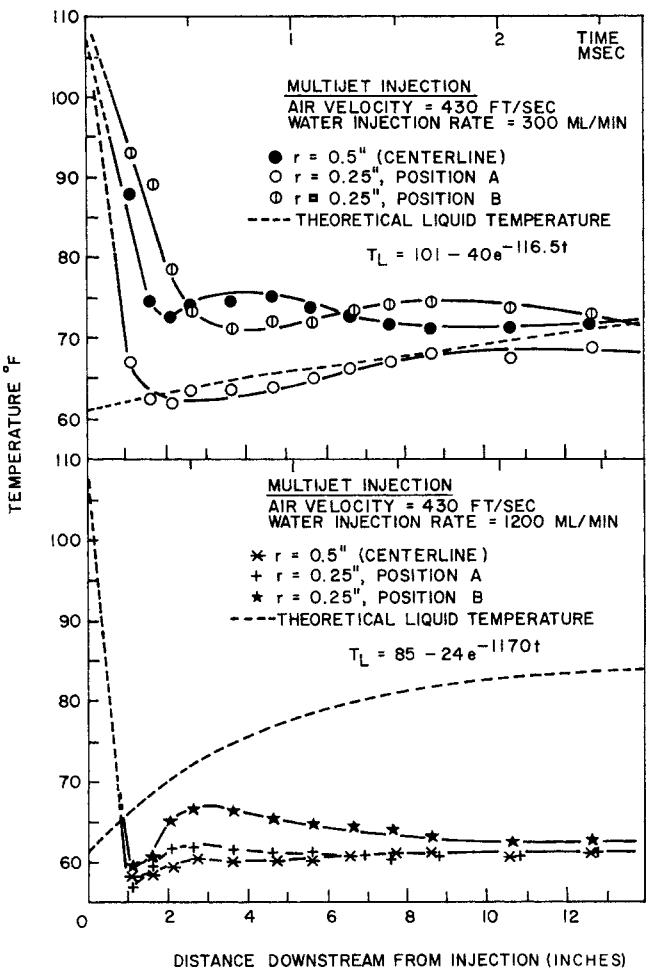


Fig. 16a. Measured temperature and theoretical liquid temperature, multijet injection.

periphery of the tube.

In the case of the three concentric tube removal probe modeled after the design of Benedict (8), the temperature measurements were variable and without apparent meaning. The probe was unsuccessful in obtaining a true gas temperature even in the relatively sparse sprays obtained by annular injection and the low airstream velocity.

The shielded thermocouple, two-phase temperature probe proved to be successful in obtaining some sort of local temperatures in the dense sprays. The measured temperature was most probably either a local liquid temperature in the case of dense sprays or a combination local liquid-gas temperature in sparse sprays.

Figures 16*a* and *b* show a comparison of experimentally measured temperature and theoretical liquid temperature calculated by using Equation (15).

Figure 16*a* (multijet) indicates the possibility that the temperature probe was measuring liquid rather than gas temperature, especially for the 300 ml./min. water injection rate. At 1,200 ml./min., the theoretical liquid temperature was higher than the temperature measured. This could be due to evaporation of water on the probe. The wet bulb temperature of the air was 57.5°F., and the experimentally measured temperature a short distance from injection is very close to this value and rises thereafter. A liquid temperature could be experimentally measured down as far as the wet bulb temperature of the air.

For the annular injection case (Figure 16*b*), it appears that the probe was indicating spray liquid temperature at the liquid injection rate of 1,200 ml./min. At the water injection rate of 300 ml./min., the experimentally measured probe temperature was higher than the theoretical liquid temperature, possibly because the probe was indicating a temperature somewhere between the gas and liquid temperatures. It should be remembered that at low liquid rates and annular injection, the liquid/gas mass ratio is quite small (in this case, $R^* = 0.035$), and the probe is less likely to stay perpetually wet.

One other anomaly was noted. The minimum probe temperature measured in the case of 1,200 ml./min. multijet injection into 430 ft./sec. air, very close to injection, was lower than the inlet water temperature. This could be explained as a wet probe with rapid evaporation, a condition which would bring the temperature down to the wet bulb temperature. The minimum temperature was very close to the wet bulb temperature, additional evidence that a water temperature rather than a gas temperature was being measured.

Overall, the evidence leads one to believe that a gas temperature was never measured in a spray by using the shielded tip, temperature probe. In some cases, such as the multijet injection and the high air velocity, a liquid temperature was probably measured. In other cases, such as the annular injection, high velocity, a temperature somewhere between the gas temperature and the liquid temperature was probably measured.

With the experimental apparatus used, it was impossible to generate conditions approximating those encountered in a high temperature spray quench ($\Delta T_G/\Delta T_L$ $10^2$-$10^3$). Therefore, only low temperature spray quenching

was investigated experimentally.

As was noted in the theoretical development of high and low temperature spray quenching, the quench time is proportional to the quantity $(d^2_{32}/R^*)$ in both cases. Since the Nukiyama-Tanasawa correlation came the closest to predicting the median drop diameters encountered in the study, it seems worthwhile to seek a minimum value for the quantity $(d^2_{32}/R^*)$ with respect to $R^*$. The Nukiyama/Tanasawa (*11*) correlation, Equation (23), can be written in the form

$$d_{32} = \lambda + \psi(R^*)^{1.5} \tag{24}$$

where

$$\lambda = \frac{585}{v_G}\sqrt{\frac{\sigma_L}{\rho_L}} \tag{25}$$

and

$$\psi \doteq 597\left(\frac{\mu_L}{\sqrt{\sigma_L \rho_L}}\right)^{0.45}\left(\frac{1{,}000\,\rho_G}{\rho_L}\right)^{1.5} \tag{26}$$

Squaring each side of Equation (24) and dividing through by $R^*$, we get an expression for $d^2_{32}/R^*$ in terms of $R^*$:

$$\frac{d^2_{32}}{R^*} = \frac{\lambda^2}{R^*} + 2\lambda\psi R^{*0.5} + (\psi R^*)^2 \tag{27}$$

The first derivative of this expression, set equal to 0, gives a possible critical $R^*$ for a minimum $(d^2_{32}/R^*)$:

$$\left\{\frac{d\left(\frac{d^2_{32}}{R^*}\right)}{dR^*}\right\}_{R^*=R^*\text{critical}} = \frac{\lambda\psi}{\sqrt{R^*_{\text{critical}}}} + 2\psi^2 R^*_{\text{critical}} - \left(\frac{\lambda}{R^*_{\text{critical}}}\right)^2 = 0 \tag{28}$$

If we assume the following physical properties which are typical for the conditions encountered in the experiments

$v_G$ = 430 or 200 ft./sec. which is 141 or 65.7 *m./sec.*
$\sigma_L$ = 72 dynes/cm.
$\mu_L$ = 0.0085 poise
$\rho_L$ = 1 g./cc.
$\rho_G$ = $1.18 \times 10^{-3}$ g./cc.

then

$\lambda$ = 82 for $v_G$ = 200 ft./sec.
$\lambda$ = 38 for $v_G$ = 430 ft./sec.
$\psi$ = 34

By using the above values in Equation (28), a minimum value for the group $(d^2_{32}/R^*)$ can be found. At an airstream velocity of 200 ft./sec., the Nukiyama-Tanasawa correlation predicts a minimum value of $(d^2_{32}/R^*)$ at $R^* \approx 1.2$, and at an airstream velocity of 430 ft./sec., the minimum $(d^2_{32}/R^*)$ occurs at $R^* \approx 0.7$.

An interesting sidelight of the development of liquid temperature profiles by the use of Equation (15), which is supported by the data in the selected cases, is the strong dependence of the shape of the liquid temperature-time curve on the volume diameter mean diameter $d_{31}$. The equation has the form

$$\frac{T_L - \tau_L}{T_{Lo} - \tau_L} = e^{\beta\left(\frac{1}{d^2_{13}}\right)t} \tag{29}$$

where

$$\beta = f(c_{pL}\, c_{pG}, R^*, k_s, N_{Nu}, \rho_L)$$

This strong dependence on $d_{31}$ may possibly be the basis for a method of obtaining an estimate of $d_{31}$ by measuring the liquid temperature of a spray in a hot gas as a function of time (distance downstream).

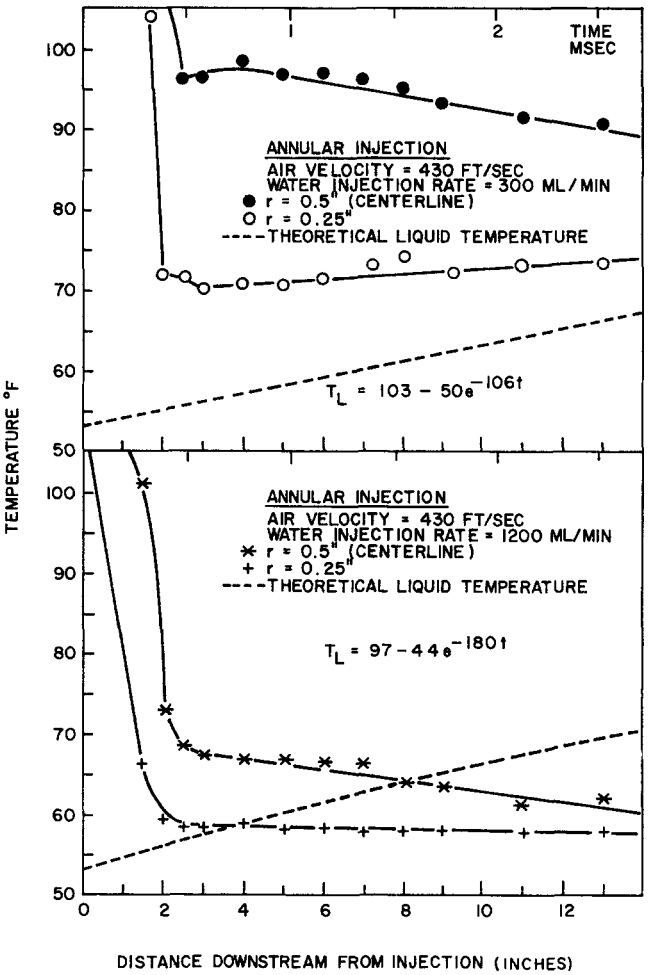


**Fig. 16b. Measured temperature and theoretical liquid temperature, annular injection.**

The conclusions reached with respect to temperature profiles are:

1. A concentric removal type of temperature probe proved successful in providing a dry gas stream (no suspended water) extracted from a spray but did not give an accurate indication of the air temperature within the spray because of cooling between the point of extraction and the point of temperature measurement. This was true in sprays with $R_c \geq 0.001$.

2. A shielded thermocouple temperature probe proved successful in obtaining local measurements of temperature which, after analysis, most probably is a liquid temperature in dense sprays ($R_c > 0.1$) and a combination liquid-gas temperature in less dense sprays ($0.01 < R_c < 0.10$).

3. For a low temperature quench, where the change in liquid temperature is of about the same order of magnitude as the change in gas temperature, the measurement of either the gas or the liquid temperature can be used to follow the quenching process.

4. Theoretical analysis of a low temperature quenching process yields the same general results as the development of a high temperature quenching process (where change in liquid temperature is negligible compared with the change in gas temperature). In both cases, the cooling or quenching rate is directly proportional to $R^*$ and inversely proportional to the square of the volume diameter mean drop size.

5. From the experimental data taken on liquid temperatures and comparison with the theoretical liquid temperatures calculated, it seems possible to achieve spray quench times of the order of milliseconds as predicted by the mathematical models for high and low temperature spray quenching, from a knowledge of real values of liquid/gas mass ratios and drop size in the sprays.

## OVERALL CONCLUSIONS

1. A multijet type of injection is superior to annular slot injection in practically every respect. In general, a multijet injector provides a more uniform liquid distribution in the spray, lower wall film flow rates (hence more water suspended), and approximately the same volume surface or Sauter mean diameter as an annular slot injector operating at the same conditions.
2. For maximum cooling or quenching, a multijet injector operating with a high airstream velocity and at a high liquid injection rate should be used. Sprays of liquid/gas mass ratio as high as 0.25 can be obtained by multijet liquid injection into a high velocity gas stream.
3. The drop size of such a spray quench can be predicted, to within 25%, by application of the Nukiyama-Tanasawa equation to these dense sprays. Sauter mean diameters as low as 45$\mu$ were obtained at liquid/gas mass ratios of 0.25.
4. Quench times can be predicted by Equation (10) and indicated quench times of the order of $10^{-3}$ sec. were obtained experimentally.


## ACKNOWLEDGMENT

Dr. Jan J. Laskowski wishes to thank the National Science Foundation for support in the form of a summer fellowship.


## NOTATION

A.E. = atomization efficiency, lb. water suspended/lb. water injected.
$C$ = Nusselt constant, defined by Equation (5), dimensionless
$c_p$ = heat capacity at constant pressure, B.t.u./(lb.$_m$) (°F.)
$c_v$ = heat capacity at constant volume, B.t.u./(lb.$_m$) (°F.)
$D$ = characteristic diameter, ft.
$D_j$ = characteristic dimension of liquid injector, ft.
$d_{VMD}$ = volume median droplet diameter, ft.
$d_{21}$ = surface diameter mean diameter, ft.
$d_{31}$ = volume diameter mean diameter, ft.
$d_{32}$ = volume surface or Sauter mean diameter, ft.
$g_c$ = Newton's law conversion factor, (lb.$_m$)(ft.)/(lb.$_f$)(sec.$^2$)
$h_c$ = convective heat transfer coefficient, B.t.u./(sq.ft.)(hr.)(°F.)
$K_1$, $K_2$ = constants, defined by Equations (20) and (21), dimensionless
$k$ = thermal conductivity, (B.t.u.)(ft.)/(sq.ft.)(hr.)(°F.)
$N_{Ma}$ = Mach number = $v/v_{so}$ (gas-velocity after the converging nozzle/speed of sound at the same conditions), dimensionless
$N_{Nu}$ = Nusselt number = $hD/k$ or $UD/k$, dimensionless
$N_{Pr}$ = Prandtl number = $c_p\mu/k$, dimensionless
$N_{Re}$ = Reynolds number = $Dv\rho/\mu$, dimensionless
$Q$ = volumetric flow rate, cu.ft./hr.; $Q_A$ = of gas, $Q_L$ = of liquid
$R$ = overall liquid/gas mass flow ratio, lb. water/lb. air
$R_c$ = liquid/gas mass ratio of spray, computed by correcting $R$ for the wall film flow rate, lb. water/lb. air
$R^*$ = liquid/gas mass ratio of spray assuming liquid is uniformly distributed, lb. water/lb. air
$S$ = specific interfacial surface area of a spray per unit mass of gas, sq.ft./lb. air
$T$ = temperature, °F.
$T_f$ = gas temperature after the converging nozzle, °F.
$T_{wbt}$ = wet bulb temperature, °F.
$T_{bp}$ = boiling point temperature, °F.
$t$ = time, sec.
$t_e$ = quench time, defined by Equation (11), sec.
$U$ = overall heat transfer coefficient, B.t.u./(sq.ft.)(hr.)(°F.)
$v$ = velocity, ft./sec.
$v_L$ = velocity of liquid jet, ft./sec.
$v_{so}$ = velocity of sound, ft./sec.
$x$ = characteristic length or diameter, ft.

### Greek Letters

$\beta$ = $f(c_{pL}, c_{pG}, R^*, k_s, N_{Nu}, \rho_L)$, defined by Equation (29)
$\delta$ = turbulent boundary-layer thickness, ft.
$\kappa$ = specific heat ratio = $c_p/c_v$, dimensionless
$\mu$ = viscosity, lb.$_m$/(ft.)(sec.)
$\rho$ = density, lb.$_m$/cu.ft.
$\sigma$ = surface tension or standard deviation, lb.$_f$/ft. or dimensionless
$\sigma_g$ = relative standard deviation, dimensionless
$\sigma_L$ = surface tension, dynes/cm.
$\tau_G$ = equilibrium temperature, defined by Equation (18), °F.
$\tau_L$ = equilibrium temperature, defined by Equation (16), °F.
$\lambda$, $\psi$ = groupings of physical properties, see Equations (25) and (26)

### Subscripts

$G$ = gas phase
$L$ = liquid phase
$d$ = diameter
$o$ = initial condition
$s$ = surface

## LITERATURE CITED


1. Eckert, E. R. G., and R. M. Drake, Jr., "Heat and Mass Transfer," 2 ed., p. 250, McGraw-Hill, New York (1959).
2. Spalding, D. B., "Some Fundamentals of Combustion," p. 73, Butterworths, England (1955).
3. Marshall, W. R., Jr., *Chem. Eng. Progr. Monograph Ser. No. 2*, **50**, 52 (1954).
4. Gurney, H. P., and J. Lurie, *Ind. Eng. Chem.*, **15**, 1170 (1923).
5. Streeter, V. L., "Fluid Mechanics," 3 ed., p. 255, McGraw-Hill, New York (1962).
6. Laskowski, J. J., Ph.D. thesis, Univ. Minn., Minneapolis (July, 1968).
7. Ranz, W. E., and C. Hofelt, Jr., *Ind. Eng. Chem.*, **49**, 288 (1957).
8. Benedict, R. P., *Trans. Am. Soc. Mech. Engrs.*, **A85**, 245 (July, 1963).
9. Schlichting, H., "Boundary Layer Theory," 4 ed., p. 537, McGraw-Hill, New York (1960).
10. Gill, L. E., G. F. Hewitt, and J. W. Hitchon, *AERE Report R-3955*, Chemical Engineering Division, Atomic Energy Research Establishment, Harwell, Berkshire, U.K. (1963).
11. Nukiyama, S., and Y. Tanasawa, *Trans. Soc. Mech. Engrs. (Japan)*, **4**, 14, 15, 86, 138 (1938); **5**, 18, 63, 68 (1939); **5**, 22, 23, II-7, II-8 (1940).



*Manuscript received November 18, 1968; revision received February 4, 1969; paper accepted February 7, 1969.*